Journal of the Korean Ceramic Society
Vol. 49, No. 1, pp. 29~36, 2012.

http://dx.doi.org/10.4191/kcers.2012.49.1.029

Oxygen Potential Gradient Induced Degradation of Oxides

Manfred Martin***,†

**Institute of Physical Chemistry, RWTH Aachen University, 52056 Aachen, Germany*
***WCU Hybrid Materials Program, Seoul National University, Seoul 151-744, Korea*

(Received December 14, 2011; Revised January 11, 2012; Accepted January 12, 2012)

ABSTRACT

In many applications of functional oxides originally homogeneous materials are exposed to gradients in the chemical potential of oxygen. Prominent examples are solid oxide fuel cells (SOFCs) or oxygen permeation membranes (OPMs). Other thermodynamic potential gradients are gradients of electrical potential, temperature or uni-axial pressure. The applied gradients act as generalized thermodynamic forces and induce directed fluxes of the mobile components. These fluxes may lead to three basic degradation phenomena of the materials, which are kinetic demixing, kinetic decomposition, and morphological instabilities.

Key words* : *Oxygen potential gradient, Degradation, Kinetic demixing, Kinetic decomposition, Morphological instability

1. Introduction

Conversion of energy from chemically stored energy to electrical energy and clean combustion of fossil fuels belong to the most challenging tasks of our modern society. Important technologies in both fields are Solid Oxide Fuel Cells (SOFCs)[1] and Oxygen Permeation Membranes (OPMs).[2] In both cases an oxide (being a solid electrolyte for SOFCs and a mixed ionic electronic conductor for OPMs) is exposed to an external oxygen potential gradient that drives oxygen ions (SOFC) or the chemical component oxygen (OPM) through the oxide. Degradation phenomena that appear as a result of the applied oxygen potential gradient, the resulting fluxes of ions and electrons, and the following compositional changes are crucial for the long-term stability and lifetime of the devices. There are, of course many more applications where an originally homogeneous material is exposed to a thermodynamic potential gradient, which can be a gradient of temperature, chemical potential of one or more elements, electrical potential or uni-axial pressure. Examples are tarnishing layers on metallic materials[3,4] which act as corrosion protection, thermal barrier coatings[5] acting as heat shield, or electronic devices such as Multi Layered Ceramic Capacitors (MLCCs) exposed to high voltages.[6] The applied gradients act as a generalized thermodynamic forces, and induce directed fluxes of the mobile components. These fluxes can lead to three basic degradation phenomena of the materials.

i. During so-called kinetic demixing the multicomponent material, which was originally chemically homogeneous, becomes chemically inhomogeneous.
ii. During so-called kinetic decomposition the formation of new phases may take place, i.e. the initially single phase material may decompose into new phases.
iii. The original morphology of the material may become unstable and a new morphology may be established (morphological instability).

It must be emphasized that all three phenomena have a purely kinetic origin, i.e. if the applied thermodynamic potential gradient is removed the directed fluxes will disappear, and due to diffusion processes the material will become again homogeneous, the new phases will disappear, and the new morphology may become unstable and the old one may be re-established.

In this article, some theoretical considerations on the thermodynamics and kinetics of the above degradation processes as well as experimental results for model systems will be reviewed. This review is based on more comprehensive treatments in references.[7,8] The class of materials will be limited to oxides. Due to their physical and chemical properties oxides are used in many technical applications, such as tarnishing layers on metallic alloys,[3] ZrO_2-layers in thermal barrier coatings,[5] Y_2-O_3-doped ZrO_2 (YSZ) being the solid electrolyte and $(La,Sr)MnO_{3-\delta}$ being the cathode material in solid oxide fuel cells (SOFC)[9] or $(Ba,Sr)(Co,Fe)O_{3-\delta}$ as mixed conductor in oxygen separation membranes.[2]

To discuss the very principle of electrochemical potential gradient induced degradation, we will consider here quasi-binary oxides, $(A_{1-x}B_x)O$. These oxides have four thermodynamic degrees of freedom, which are the pressure, p, the temperature, T, the composition, x, and the chemical potential of oxygen, $\mu_{O_2} = \mu^0_{O_2} + R\,T\ln(p_{O2}/p^0)$ (p_{O2} is the oxygen partial pressure and $p^0 = 1$ bar the standard pressure). If such an oxide is exposed to a chemical potential gradient (without any gradient in total pressure, p, or temperature, T), e.g. to an oxygen

†Corresponding author : Manfred Martin
E-mail : martin@rwth-aachen.de
Tel : +49-241-8094712 Fax : +49-241-8092128

potential gradient, then gradients of the chemical potentials of the chemical components A and B are induced as a consequence of the Gibbs-Duhem relation, $x_A d\mu_A + x_B d\mu_B + x_O d\mu_O = 0$ (Fig. 1(a)). These thermodynamic forces generate fluxes of all mobile components, i.e. cations, A^{2+} and B^{2+}, oxygen ions, O^{2-}, and electrons, e', and electron holes, h$^{\cdot}$, Cations and oxygen ions are assumed to be mobile by means of vacancies V_{cation} and V_O in the respective sublattices, and the corresponding fluxes are coupled, $j(A^{2+}) + j(B^{2+}) + j(V_{cation}) = 0$ and $j(O^{2-}) + j(V_O) = 0$ (Fig. 1(b)). We note that oxygen only permeates through the oxide from the high to the low oxygen potential side (depending on the magnitude of the electronic transference number) and does not cause any direct degradation (Fig. 1(b)).

The situation is, however, different concerning the transport of cations. If cations and cation vacancies arrive at the crystal surfaces chemical reactions have to take place. At the high-p_{O2} side, cations, A^{2+} (and B^{2+}), are oxidized by oxygen, O2(g), from the gas phase, and cation vacancies, V_{cation}, and new lattice molecules, AO (and BO), of the oxide are produced. At the low-p_{O2} side a reduction takes place, i.e. cation vacancies are annihilated, and oxide molecules are reduced to cations and oxygen.

$$A^{2+} + \frac{1}{2}O_2(\text{gas}) + 2e' \underset{\text{reduction}}{\overset{\text{oxidation}}{\rightleftarrows}} V_{cation} + AO,$$

$$B^{2+} + \frac{1}{2}O_2(\text{gas}) + 2e' \underset{\text{reduction}}{\overset{\text{oxidation}}{\rightleftarrows}} V_{cation} + BO$$

As a consequence of these reactions both oxide surfaces shift to the side of higher oxygen potential with a velocity $v_{surface}$. If both cations have different mobilities, the originally homogeneous oxide will become inhomogeneous, as depicted in Fig. 1(b). The faster of the two components A and B becomes enriched at the high-p_{O2} side while the slower component is left behind and becomes enriched at the low-p_{O2} side (kinetic demixing). In summary, the external oxygen potential gradient causes: (a) a directed flux of cation vacancies, $j(V_{cation}) = -j(A^{2+}) - j(B^{2+})$, from the high to the low oxygen potential side of the oxide, (b) a drift motion of both crystal surfaces towards the high-p_{O2} side, and (c) demixing of the cations with enrichment of the faster cation at the high-p_{O2} side. The demixing will start at the crystal surfaces, and after some time a steady state will be reached where both crystal surfaces move with the same, constant velocity, and the demixing profile has become stationary (relative to the moving surfaces).

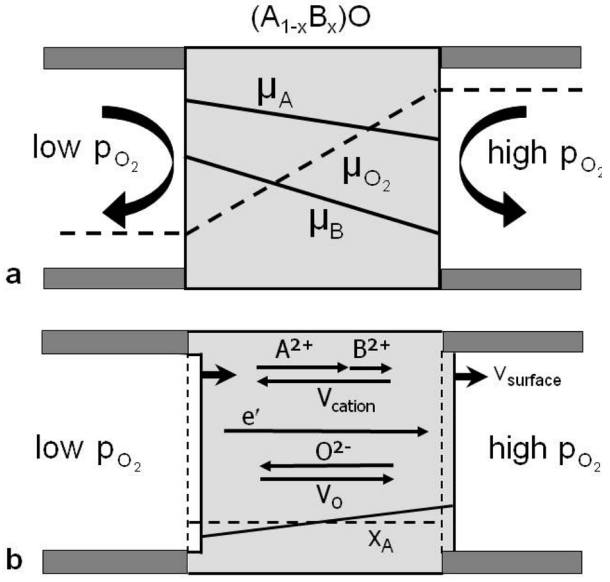

Fig. 1. Schematic experimental setup of an oxide that is exposed to an oxygen potential gradient. (a) Chemical potential gradients of the chemical components A, B, and O. (b) Fluxes of cations, A^{2+} and B^{2+}, cation vacancies, V_{cation}, oxygen ions, O^{2-}, oxygen vacancies, V_O, and electrons, e'. Also shown are the demixing profile of the faster component A and the shift of the crystal surfaces moving with the velocity $v_{surface}$.

The paper is organized as follows: In chapter 2 the formal treatment of steady state demixing in a general electrochemical potential gradient will be reviewed. Chapter 3 treats demixing in an oxygen potential gradient. At first homovalent solid solutions and then heterovalently doped oxides will be considered. The important cases of oxygen ion conductors and mixed oxygen ion and electronic conductors will be discussed separately. Finally, in chapter 4 the morphological stability of the surfaces and pore motion will be treated.

2. Formal Treatment of Steady State Demixing in an Electrochemical Potential Gradient

According to linear, irreversible thermodynamics[10] the driving forces for the motion of charged species (index k) are the gradients of their electrochemical potentials, $\eta_k = \mu_k + z_k \cdot F \cdot \Phi$, where μ_k is the chemical potential, z_k the charge number, F Faraday's constant, and Φ the electric potential.

The corresponding equations for cations, $A^{z_{A+}}$ and $B^{z_{B+}}$, and electrons, e' , and electron holes, h$^{\cdot}$, are:

$$j(k) = -\sum_l L_{kl} \nabla\eta(l) \qquad (k, l = A^{z_{A+}}, B^{z_{B+}}, e', h^{\cdot}) \tag{2}$$

The quantities L_{kl} are the Onsager transport coefficients.[19] In the steady state, both cations are moving with the same velocity, v_{stat}, relative to the immobile oxygen sublattice of the oxide. Since the fluxes can always be written as the product of a velocity and a concentration, $j_k = v \cdot c_k$, the steady state condition is given by:

$$v_{stat} = \frac{j(A^{z_{A+}})}{c_A} = \frac{j(B^{z_{B+}})}{c_B} \tag{3}$$

From Eqs. (2) and (3) we obtain the 'demixing equation' that relates the two forces $\nabla\mu_A$ and $\nabla\mu_B$ (corresponding to the chemical components $A \rightleftarrows B^{z_{A+}} + z_A e'$ and $B \rightleftarrows B^{z_{B+}} z_{B+} \cdot e'$), and the force on the electrons, $\nabla\eta(e')$ (due to the internal electronic equilibrium we have $\nabla\eta(e') + \nabla\eta(h^{\cdot}) = 0$):

$$\nabla\mu_B = \Psi \cdot \nabla\mu_A - \Gamma \cdot \nabla\eta(e') \tag{4}$$

The functions Ψ and Γ are given by

$$\psi = \frac{x_B \cdot L_{AA} - x_A \cdot L_{BA}}{x_A \cdot L_{BB} - x_B \cdot L_{AB}} \qquad \Gamma = \frac{x_B \cdot z_A^{eff} \cdot L_{AA} - x_A \cdot z_B^{eff} \cdot L_{BB}}{x_A \cdot L_{BB} - x_B \cdot L_{AB}} \quad (5)$$

where z_A^{eff} and z_B^{eff} are the so-called effective charges of A and B:

$$z_A^{eff} = z_A + \frac{L_{Ae}}{L_{AA}} + z_B \frac{L_{AB}}{L_{AA}}, \qquad z_B^{eff} = z_B + \frac{L_{Be}}{L_{BB}} + z_A \frac{L_{AB}}{L_{BB}} \quad (6)$$

The effective charges contain the diagonal coefficients and the cross-coefficients of the Onsager transport matrix. The former describe the direct influence of the forces while the latter express the flux coupling between different mobile components. For example, L_{AB} describes the flux of $A^{z_{A+}}$ due to the force $\nabla\eta(B^{z_{B+}})$ (see Eq. (2)), and, because of the Onsager relation, $L_{AB} = L_{BA}$, also the opposite effect, i.e. the flux of $B^{z_{B+}}$ due to the force $\nabla\eta(A^{z_{A+}})$. This means, that the difference between the effective charges, z_i^{eff}, and the formal charges, z_i, has a purely kinetic origin.[11]

3. Steady State Demixing in an Oxygen Potential Gradient

If only an external oxygen potential gradient is applied there will be no net electric current, i, through the oxide (ambipolar diffusion). Then, the gradient of the electrochemical potential of the electrons in Eq. (4), $\nabla\eta(e')$, can be computed from the condition $i = 0$. As long as the oxide under consideration is a good semiconductor, the transport coefficients of electrons and electron holes are much larger than all other transport coefficients, L_{ee}, $L_{hh} >> L_{ii}$, and the corresponding forces are approximately zero, $\nabla\eta(e') = \nabla\eta(h^{\cdot}) \approx 0$. Thus, the demixing equation (4) simplifies to $\nabla\mu_B = \Psi\nabla\mu_A$, and only the parameter Ψ determines the demixing behavior. Kinetic demixing induced by an external electric potential gradient will not be discussed in this article, but we note that the parameter Γ in Eq. (4) then becomes important.[12,13]

3.1. Homovalent solid solutions

In a homovalent solid solution of AO and BO the Onsager cross coefficients may be neglected and the diagonal coefficients are given by $L_{kk} = D_k c_k / RT$ (D_k and c_k are the diffusion coefficient and concentration of species k), Ψ in Eq. (5) simplifies to $\Psi = D_A/D_B$, and the demixing equation (4) to $\nabla\mu_B = (D_A/D_B)\nabla\mu_A$. Using the equilibria $A + \frac{1}{2}O_2(g) \leftrightarrows AO$ and $B + \frac{1}{2}O_2(g) \leftrightarrows BO$ and as-suming an ideal solid solution of AO and BO, we obtain $\nabla\mu_A + \frac{1}{2}\nabla\mu_{O2} = \nabla\mu_{AO} = RT\nabla\ln x_A$ (x_A is the molar fraction of A) and an analogous expression for B, $\nabla\mu_B + \frac{1}{2}\nabla\mu_{O2} = \nabla\mu_{BO} = RT\nabla\ln x_B$.

With these relations Eq. (4) can finally be written as:

$$\left(\frac{1}{1-x_A} + \frac{D_A}{D_B}\cdot\frac{1}{x_A}\right)\cdot RT\nabla x_A = \left(\frac{D_A}{D_B} - 1\right)\cdot\frac{1}{2}\nabla\mu_{o_2} \quad (7)$$

Eq. (7) shows that the ratio D_A/D_B determines whether there is kinetic demixing ($\nabla x_A \neq 0$) and at which side of the oxide component A becomes enriched . If both components have the same diffusion coefficient, $D_A/D_B = 1$, there will be no demixing, $\nabla x_A = 0$. If $D_A/D_B > 1$ (A is the faster component), ∇x_A has the same sign as the oxygen potential gradient, $\nabla\mu_{o_2}$, i.e. A becomes enriched at the high-p_{O2} side. If, on the other hand, B is the faster component, $D_A/D_B < 1$, A becomes enriched at the low-p_{O2} side. As shown first by Schmalzried et al.,[14] the demixing profile is then obtained by integration of Eq. (7) with appropriate boundary conditions. The resulting theoretical demixing profiles are in good agreement with the experimentally found demixing profiles in the solid solution CoO-MgO where Co is the faster component. As expected, strong enrichment of Co was found at the high-p_{O2} side of the material.

3.2. Heterovalently doped oxides

In a heterovalently doped oxide AO that is e.g. doped with B_2O_3, the positive excess charge of the dopant cation B^{3+} (compared to the host cation A^{2+}) may result in the formation of charge compensating cation vacancies, V_{cation}. Then the oxide solid solution, $(A_{1-x}B_x)O$, can no longer be treated as an ideal solution. As shown in detail in Ref.,[7] in a dilute oxide, $A_{1-x}B_xO$ ($x << 1$), the flux of the dopant, B, can be written as

$$j_B = -D_B\cdot\nabla c_k - j_{v_{cation}}\cdot\frac{L_{BB}}{L_{AA}}\cdot\left(\rho + \frac{L_{BA}}{L_{BB}}\right) \quad (8)$$

The dimensionless quantity ρ contains all physical correlation effects and is of the order of 1. Eq. (8) shows that the dopant flux consists of two terms, a pure diffusion term, $-D_B\nabla c_B$, characterized by the dopant diffusion coefficient, D_B ($= L_{BB}RT/c_B$), and a drift term, that is proportional to the directed vacancy flux, jv_{cation}. The direction of the drift term, which determines at which side of the sample the dopant becomes enriched, depends crucially on the sign and magnitude of the non-diagonal Onsager coefficient L_{BA}. In heterovalently doped oxides, e.g. $AO(+B_2O_3)$, solute-vacancy interactions might result in a non-vanishing and negative cross term L_{AB}. These interactions are caused by the Coulomb interactions between the excess charges of the defects and elastic effects.[15,11] The interaction may be weak (as is expected for homovalent dopant ions) or stronger (for heterovalent dopant ions). If the interaction is weak, dopant ions and vacancies do not form bound pairs but drift in opposite directions. For strong attractive interaction, on the other hand, dopant ions and vacancies form bound pairs, and the dopant ions drift in the same direction as the vacancies.

This qualitative picture is confirmed by a microscopic diffusion model that considers nearest-neighbor interactions. The so-called five-frequency model[16] uses five exchange frequencies of vacancies and ions (Fig. 2): ω_0 and ω_1 for exchange of vacancies with solvent ions in the pure crystal (i.e. far away from the dopant ion) and in the nearest neighborhood of the solute ion; ω_3 for vacancy jumps, which dissociate a dopant-vacancy pair; ω_4 which creates a new pair; and ω_2 for exchange of a vacancy and a solute ion.

ω_3 and ω_4 are coupled by the condition of detailed balance, $\omega_4/\omega_3 = \exp(-\Delta g_{pair}/RT)$, where Δg_{pair} is the binding Gibbs energy of the solute-vacancy pair. Within this model the

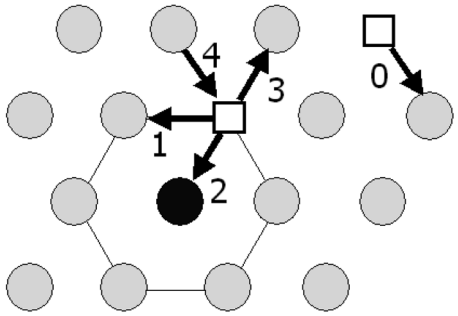

Fig. 2. Five-frequency model of dopant diffusion (grey circle = matrix cation A, black circle = dopant cation B, open square = cation vacancy, $\omega_k (k = 0\text{-}4)$ = exchange frequencies of vacancies and cations (see text)).

transport coefficients L_{ij} (i, j = A, B) are known exactly.[17] While the ration L_{BB}/L_{AA} is always positive the ratio L_{AB}/L_{BB} may become negative for strong dopant-vacancy binding. A detailed analysis using a defect model for the doped oxide[18] shows that the gradient of the dopant profile, ∇x_B, can be written as

$$\nabla \ln x_B = \kappa \nabla \ln p_{O2} \quad (9)$$

where κ is again a function of the demixing parameter Ψ in Eq. (5). The sign of κ decides whether the dopant becomes enriched at the high-p_{O2} side (κ > 0) or at the low-p_{O2} side (κ < 0). κ depends on the (dimensionless) impurity-vacancy binding energy, $\varepsilon = |\Delta g_{pair}|/RT$, and the jump frequency ratio $t = \omega_2/\omega_0$. In Fig. 3 the ε-t plane is shown with the boundary line on which the parameter κ wavishes, thereby separating parameter regions with enrichment of B at the high- or low-p_{O2} sides. If ω_2 is large compared to ω_0, then κ is positive, but only for moderate binding energies ε < 1. This mean that the faster component B enriches at the high-p_{O2}, side as expected. If, however. the binding energy becomes larger, κ becomes negative for all values of ω_2/ω_0 and B becomes always enriched at the low-p_{O2} side. This behavior can be understood as follows: for large ε the cation vacancy is strongly bound to the dopant, resulting in a long lifetime of the pair and a negative Onsager cross coefficient L_{AB}, *i.e.* the dopant drift flux due to the oxygen potential gradient is directed to the low - p_{O2} side, as the cation vacancy flux (Eq. (8)).

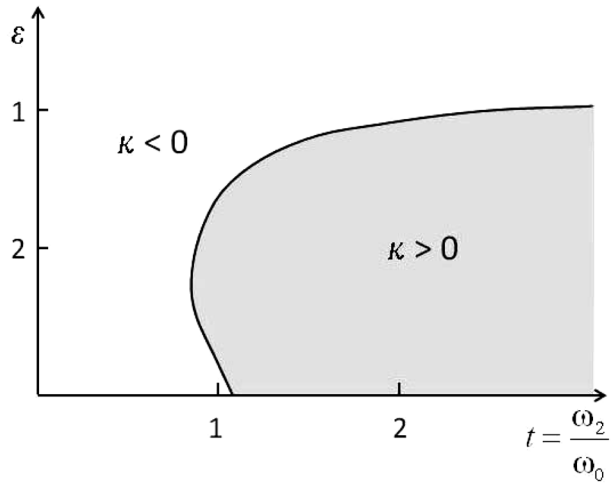

Fig. 3. Demixing regions in the ε-t plane for an average dopant fraction $x_B = 0.02$. $\varepsilon = |\Delta g_{pair}|/R\ T$ is the dimensionless dopant-vacancy binding energy, $t = \omega_2/\omega_0$, and $\kappa = d\ln x_B/d\ln p_{O2}$.

Demixing experiments with Ga_2O_3-doped CoO[18] show enrichment of Ga at the low oxygen potential side (Fig. 4), which corresponds to the region κ < 0 in Fig. 3. As tracer diffusion of Ga is slightly slower than that of Co[19] this behavior indicates strong dopant-vacancy binding. The combined analysis of the tracer diffusion data and the demixing experiment yields a dopant-vacancy binding energy of ~0.4 eV and a ratio $L_{CoGa}/L_{GaGa} = -1.7$, confirming that the drift flux in Eq. (8) is directed to the low oxygen potential side.

3.3. Kinetic decomposition

If during the demixing process the stability field of the material is left, decomposition of the material and the formation of new phases might take place (kinetic decomposition). First Schmalzried and Laqua[20] observed the formation of a multiphase layer in the system NiO-TiO_2 after exposure of a single phase $NiTiO_3$-crystal to an oxygen potential gradient. While (Ni,Ti)O is formed at the high oxygen potential side, TiO_2 was found at the low oxygen potential side of the crystal. The origin of this process is again the difference of the diffusion coefficients of Ni and Ti in $NiTiO_3$, but now demixing is driven to the point where the stability field of the oxide is left. Kinetic decomposition was also found for fayalite, Fe_2SiO_4, exposed to an oxygen potential gradient[21] (formation of SiO_2 and Fe_3O_4 at the low respectively high oxygen potential side). More examples will be discussed in the next chapter.

3.4. Demixing and decomposition in oxides with prevailing oxygen disorder

Demixing in an oxygen potential gradient might be important

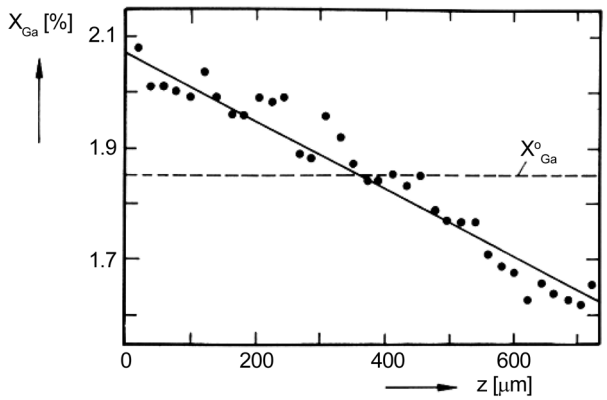

Fig. 4. Demixing profile of Ga in $(Co_{1-x}Ga_x)O$ exposed to an oxygen potential gradient ($T = 1250^oC$, $p_{O2}^{left} = 10^{-6}$ bar, $p_{O2}^{right} = 10^{-5}$ bar, $\Delta z = 725$ μm, $x^0_{Ga} = 1.85\%$, $t = 38.5$ h).[18]

also in oxygen ion conductors, such as yttria-doped zirconia (YSZ) or SrO- and MgO-doped lanthanum gallate (LSGM). When these oxides are used as electrolytes, e.g., in solid oxide fuel cells (SOFCs), oxygen ions are driven through the electrolyte due to the applied oxygen potential gradient, and simultaneously electrons are flowing through the external circuit. As soon as the cations, e.g., Zr^{4+} and Y^{3+} in YSZ, have different diffusion coefficients there will be demixing of the electrolyte. The detailed formal analysis can be found in references.[22,23] Since cation diffusion is very slow in these oxides,[24,25] steady state demixing will be reached only after rather long times. If, for example, the slowest diffusion coefficient is taken as $D = 10^{-14}$ cm^{2}s^{-1}, one obtains 15,000 years for an electrolyte thickness of 1 mm. However, for a thickness of 10 μm (which is realized in supported SOFCs[26]) the time to reach the steady state is only several years which is comparable to the desired operating times of SOFCs.

Demixing phenomena are also important in the field of oxygen permeation membranes[2] where oxygen diffusion is again much faster than cation diffusion. In contrast to SOFCs, these oxides are mixed ionic electronic conductors (MIEC), *i.e.* oxygen diffusion proceeds via ambipolar diffusion of oxygen ions and electrons (or electron holes). Most oxygen permeation membranes are composed of oxides that belong to the family of perovskites ABO_3. High oxygen diffusivity is obtained by heterovalent doping and/or the usage of transition metal oxides on the B-sites of the perovskite. Prominent examples are $(Ba,Sr)(Co,Fe)O_{3-\delta}$ (BSCF) or $(La,Sr)(Co,Fe)O_{3-\delta}$ (LSCF). In principle, the same methods as described above can be used to analyze the demixing and decomposition behavior of these materials in an applied oxygen potential gradient. There are, however, several points that render such a treatment more difficult for perovskites $(A,A')(B,B')O_{3-\delta}$ and explain why a comprehensive treatment is still missing.

i. In a perovskite, there are two cation sublattices, i.e. the A- and the B-sublattice. Depending on the diffusion coefficients of A, A', B and B', cation demixing may take place only within the A-sublattice (resulting in demixing of A and A'), only within the B-sublattice (resulting in demixing of B and B'), and in both sublattices (resulting in a change of the cation molecularity, i.e. the ratio ([A]+[A'])/([B]+[B']).
ii. In many perovskites the understanding of the defect chemistry is still poor, thus making it rather difficult to analyze the diffusion properties that depend crucially on the defect properties in detail and quantitatively.
iii. In most perovskites the stability field is rather small, *i.e.* the ratio ([A]+[A'])/([B]+[B']) can be varied only slightly around its ideal value of 1. As a consequence, kinetic decomposition will lead most often to kinetic decomposition. During this process new phases will appear but also the morphology of the membrane may change (see next chapter), rendering a quantitative treatment again more difficult.

There are several experimental reports on cation demixing and decomposition of oxides during operation as oxygen permeation membrane (OPM). Diethelm *et al.*[27] report on kinetic decomposition of $(La_{0.6}Ca_{0.4})(Fe_{0.75}Co_{0.25})O_3$ (LCFC) that was used as OPM during partial oxidation of methan at 900°C. In this relatively high oxygen potential gradient they observed on both sides of the mebrane strong compositional changes and the formation of several new phases. In a very recent study, Wang *et al.*[28] found kinetic demixing and decomposition in $La_{0.6}Sr_{0.4}Co_{0.2}Fe_{0.8}O_{3-\delta}$ oxygen-separation hollow fibre membranes, which were operated under a 0.009/0.21 bar oxygen partial pressure difference at 950°C up to 5000 h. Kinetic demixing and decomposition was observed. Secondary-phase grains were found on the air-side surface of the membranes after the long-term operation and Co and Fe enrichment as well as La depletion was found on the surface and in the bulk at the air side. Surprisingly, the oxygen permeability was not affected by the kinetic demixing and decomposition of the material even during long-term operation.

4. Morphological Stability and Pore Motion

In the previous treatment of oxides that are exposed to an oxygen potential gradient it was assumed that the initially planar and parallel surfaces of the oxide are morphologically stable during their motion, i.e. that they do not change their planar form. Only under these assumptions the diffusion phenomena in an oxygen potential gradient could be treated as a one-dimensional diffusion problem. Thus, a further degradation process of the material, the morphological stability of the oxide surfaces, must be considered. A detailed treatment of the problem can be found in references,[29,7] Here only some important results will be discussed.

The basic situation is shown in Fig. 5 where an oxide is exposed to an oxygen potential gradient and one surface is

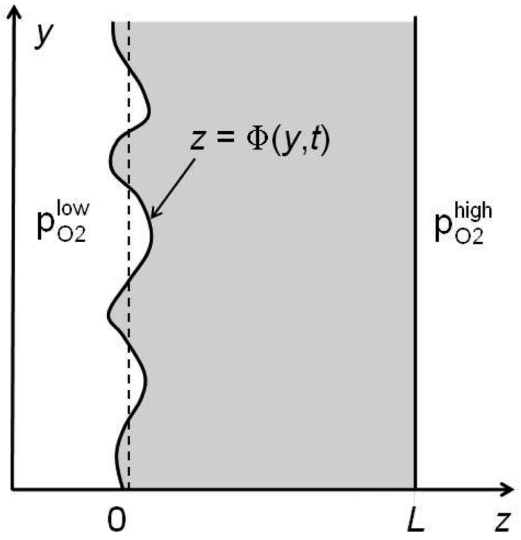

Fig. 5. Schematic representation of an oxide in an oxygen potential gradient with non-planar surface at the low-p_{O2} side. $\Phi(y, t)$ is the amplitude of the disturbance of the planar surface.

assumed to have a non-planar structure. The corresponding three-dimensional diffusion problem can be solved by means of a linear stability analysis, where it is assumed that the perturbation of the planar surface is small, i.e. $\Phi/L \ll 1$. Then it can be shown that each Fourier component $\Phi(k,t)$ of a disturbance $\Phi(y,t)$ of the planar surface grows or decays in time following an exponential growth law,

$$\Phi(k,t) = \Phi(k,0)\cdot\exp(-r(k)\cdot t). \quad (10)$$

Here $k = 2\pi/\lambda$ is the wavevector corresponding to the wavelength λ of the disturbance and $r(k)$ is the growth rate.

Fig. 6 shows the growth rates $r(k)$ for the low- and the high-p_{O2} sides of the oxide. At the low-p_{O2} side the growth rate, $r(k)$, is positive for all wave vectors, k. Thus all Fourier-components $\Phi(k,t)$ grow exponentially with time, which means that the planar crystal surface at the low-p_{O2} side (reduction) is morphologically unstable. In contrast, the growth rate at the high-p_{O2} side is always positive, i.e. this planar surface is morphologically stable. If now the stabilizing effect of the surface tension is taking into account the dispersion of the growth rate at the low-p_{O2} side changes. One recognizes that for $\sigma \neq 0$ a region exists where p(k) vecomes negative. In this region with $k > k_0 \sim \sigma^{-1/2}$ the planar surface morphologically stable due to the surface tension, σ. Instabilities appear only in a region $0 < k < k_0$ where the growth rate, r, has a maximum at $r_{max} = r_0/\sqrt{3}$. Since the Fouriercomponent of a disturbance with wave vector r_{max} has the largest growth rate, it will dominate after some time, an the initially plaanar surface should transform to a nonplanar surface with a typical dimension $\lambda_{max} = 2\pi/k_{max}$.

Figs. 7 and 8 show typical experimental results that were obtained for a single crystal of $Co_{1-\delta}O$ exposed to an oxygen potential gradient. In Fig. 7 the initial stage of the instabilities can be seen. Indentations in the form of pyramids have formed within the initially planar surface, presumably at points were

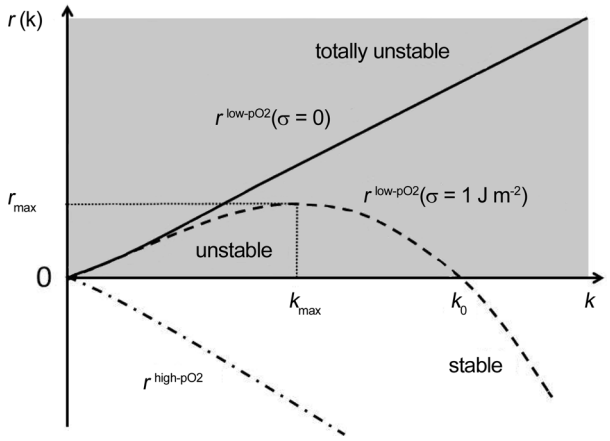

Fig. 6. Growth rates $r(k)$ of a disturbance of the planar surface at the low-p_{O2} side (for vanishing surface tension, $\sigma = 0$, solid line and for $\sigma = 1$ J m^{-2}, dashed line) and at the high-p_{O2} side (dash-dot line).

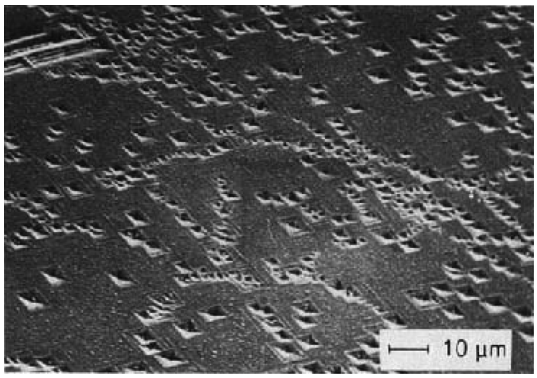

Fig. 7. Unstable surface at the low-p_{O2} side of a CoO single crystal in an oxygen potential gradient (T = 1200°C, p_{O2}(low) = $5\cdot10^{-5}$ bar, p_{O2}(high) = 0.21 bar, t = 5 h).

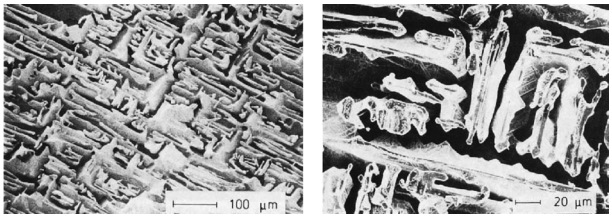

Fig. 8. Unstable surface at the low-p_{O2} side of a CoO single crystal in an oxygen potential gradient (T = 1200°C, p_{O2}(low) = $5\cdot10^{-5}$ bar, p_{O2}(high) = 0.21 bar, t = 30 h).

dislocations push through the surface resulting in an increased probability for the for mation of holes.

Starting from these "nuclei" a nearly regular new structure with a strong anisotropy forms after a longer diffusion time. Fig. 8(a) shows an overview and Fig. 8(b) an enlarged section.

The typical dimension of the new non-planar structure in Fig. 8 is about 20 µm. If the wavelength, λ_{max}, according to Fig. 6 is calculated with a typical surface tension, $\sigma = 1$ Jm^{-2} one obtains $\lambda_{max} \approx 10$ µm. Thus it seems to be possible to predict the typical wavelength of the non-planar surface with the help of the linear stability analysis and the surface tension. The actual morphology depends, however, on the anisotropy of the surface tension and can be treated theoretically by means of Monte Carlo simulations.[30]

An additional degradation effect is due to the presence of pores inside the oxide that is exposed to an oxygen potential gradient. If we assume that the pores contain a small amount of oxygen gas, they will form a short-circuit for oxygen, diffusing either through the gas phase or along the pore surface. This means that the reactions in Eq. (1) which were originally formulated for the two crystal surfaces (Fig. 1) can take place at the pore surfaces as well. However, we must now consider that the pore is a negative crystal, i.e. the oxidation reaction in Eq. (1) will take place at the pore surface that is pointing to the external low-p_{O2} side and the reduction reaction in Eq. (1) will take place at the opposite side of the pore surface. As a consequence the pore will drift to the high oxygen potential side.

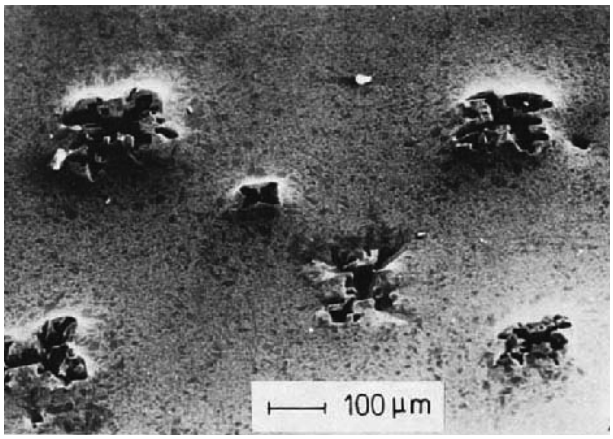

Fig. 9. Top view of the surface at the high-p_{O2} side of a CoO single crystal in an oxygen potential gradient with pores breaking through the surface.

Assuming for the sake of simplicity a spherical pore the corresponding diffusion problem can be solved[30] and the pore velocity can be calculated. The pore velocity is independent of the pore radius, i.e. there is no coalescence of pores due to a size-dependent pore velocity as observed e.g. during pore migration in a temperature gradient.[31] The calculation shows also that the pore velocity is three times larger than the velocity of the crystal surfaces, $v_{pore} = 3 \cdot v_{surface}$. Thus pores should reach the high-p_{O2} side of the oxide after some time destroying the (morphologically stable) planar surface. An example is shown in Fig. 9. Closer inspection of the pores in Fig. 9 shows that their internal surfaces exhibit similar morphologies as the oxide surfaces. The internal surface where the oxidation reaction (Eq. (1) takes place is morphologically stable, while the opposite internal surface where the reduction reaction takes place is unstable.

5. Summary

We have discussed three types of degradation mechanisms for oxides exposed to an oxygen potential gradient, kinetic demixing, kinetic decomposition, and morphological instabilities, all of which are of great significance for the application of materials. For the cation demixing in a solid solution of homovalent oxides, $(A_{1-x}B_x)O$, we have reviewed the formal analysis of the transport problem. As expected the faster cation is enriched at the high-p_{O2} side. In contrast, the demixing behavior in heterovalently doped oxides is determined by the formation of dopant-vacancy pairs. For strong binding the dopant is enriched at the low-p_{O2} side. Finally, we have discussed morphological instabilities of the oxide surfaces and the motion of pores. While a planar surface at the high-p_{O2} side is morphologically stable a planar surface at the low-p_{O2} side is unstable and develops a non-planar structure. Pores in the oxide move drift towards the high-p_{O2} side with a velocity that is three times faster than the surface velocity.

REFERENCES

1. B. C. H. Steele and A. Heinzel, "Materials for Fuel-cell Technologies," *Nature*, **414** 345-52 (2001).
2. J. Sunarso, S. Baumann, J.M. Serra, W.A. Meulenberg, S. Liu, Y.S. Lin, and J.C. Diniz da Costa, "Mixed Ionic.electronic Conducting (MIEC) Ceramic-based Membranes for Oxygen Separation," *J. Membrane Science*, **320** 13-41 (2008).
3. H. J. Grabke and M. Schutze (Eds.), Oxidation of Intermetallics, Wiley-VCH, Weinheim, 1997.
4. U. Koops, D. Hesse, and M. Martin, "High-Temperature Oxidation of CoGa: Influence of the Crystallographic Orientation on the Oxidation Rate," *J. Mater. Res.*, **17** 2489-98 (2002).
5. E. Ryshkewitch and D. W. Richerson, Oxide Ceramics, Academic, Orlando, 1985.
6. H. Kishi, Y. Mizuno, and H. Chazono, "Base-Metal Electrode-Multilayer Ceramic Capacitors: Past, Present and Future Perspectives," *Jpn. J. Appl. Phys.*, **42** 1-15 (2003).
7. M. Martin, "Transport and Degradation in Transition Metal Oxides in Chemical Potential Gradients," *Materials Science Reports*, **7** 1-86 (1991).
8. M. Martin, "Materials in Thermodynamic Potential Gradients," *J. Chem. Thermodynamics*, **35** 1291-1308 (2003).
9. A. Hammou and J. Guindet, "Solid Oxide Fuel Cells," pp 407-443 in The CRC Handbook of Solid State Electrochemistry. Ed. by P. J. Gellings and H. J. M. Bouwmeester, CRC Press, Boca Raton, 1996.
10. S.R. de Groot and P. Mazur, Non-Equilibrium Thermodynamics, North-Holland, Amsterdam, 1962.
11. J. Janek, M. Martin, and H.-I. Yoo, "Electrotransport in Ionic Crystals: I. Application of Liquid Electrolyte Theory," *Ber. Bunsenges. Phys. Chem.*, **98** 655-664 (1994).
12. O. Teller and M. Martin, "Kinetic demixing of (CoNi)O in an Electrical Field," *Solid State Ionics*, **101-103** 475-478 (1997).
13. O. Teller and M. Martin, "Steady State Demixing of Oxid Solid Solutions in an Electrical Potential Gradient," *Electrochemistry*, **68** 294-297 (2000).
14. H. Schmalzried, W. Laqua, and P.L. Lin, "Crystallic Oxide Solid Solutions in Oxygen Potential Gradients," *Z. Naturforsch.*, **34a** 192-99 (1979).
15. H.-I. Yoo, J.-H. Lee, M. Martin, J. Janek, and H. Schmalzried, "Experimental Evidence of the Interference Between Ionic and Electronic Flows in an Oxide with Prevailing Electronic Conduction," *Solid State Ionics*, **67** 317-22 (1994).
16. A.B. Lidiard, "Impurity Diffusion in Crystals (Mainly Ionic Crystals with the Sodium Chloride Structure)," *Phil. Mag.*, **46** 1218-37 (1955).
17. A. R. Allnatt and A. B. Lidiard, "Statistical Theories of Atomic Transport in Crystalline Solids," *Rep. Prog. Phys.*, **50** 373-472 (1987).
18. M. Martin and R. Schmackpfeffer, "Demixing of Doped Oxides: Influence of Defect Interactions," *Solid State Ionics*, **72** 67-71 (1994).
19. R. Schmackpfeffer and M. Martin, "Tracer Diffusion and Defect Structure in Ga-doped CoO," *Phil. Mag. A*, **68** 747-65 (1993).
20. H. Schmalzried and W. Laqua, "Multicomponent Oxides in Oxygen Potential Gradients," *Oxid. Metals*, **15** 339-53 (1981).
21. U. Brinkmann and W. Laqua, "Decomposition of Fayalite

(Fe_2SiO_4) in an Oxygen Potential Gradient at 1418 K," *Phys. Chem. Minerals*, **12** 283-90 (1985).
22. M. Martin, "Cation Demixing in an Oxygen Ion Conductor exposed to an Oxygen Potential Gradient," pp 308-316, in SOFC-VI, PV 1999-19, The Electrochemical Society Proceedings Series, Ed. by S. C. Singhal, Pennington, NJ, 1999.
23. M. Martin, "Electrotransport and Demixing in Oxides," *Solid State Ionics*, **136-137** 331-337 (2000).
24. M. Kilo, M.A. Taylor, Ch. Argirusis, G. Borchardt, B. Lesage, S. Weber, S. Scherrer, H. Scherrer, M. Schroeder, and M. Martin, "Cation self-diffusion of ^{44}Ca, ^{88}Y and ^{96}Zr in Single-crystalline Calcia- and Yttria-doped Zirconia," *J. Appl. Phys.,* **94** 7547-52 (2003).
25. O. Schulz, M. Martin, C. Argirusis, and G. Borchardt, "Cation Tracer Diffusion of ^{138}La, ^{84}Sr and ^{25}Mg in Polycrystalline $La_{0.9}Sr_{0.1}Ga_{0.9}Mg_{0.1}O_3$," *Phys. Chem. Chem. Phys.*, **5** 2308-13 (2003).
26. N. H. Menzler, F. Tietz, S. Uhlenbruck, H. P. Buchkremer, and D. Stoever, "Materials and Manufacturing Technologies for Solid Oxide Fuel Cells," *J. Mater. Sci.*, **45** 3109-135 (2010).
27. S. Diethelm, J. Sfeir, F. Clemens, J. van Herle, and D. Favrat, "Planar and Tubular Perovs-kite-type Membrane Reactors for the Partial Oxidation of Methane to Syngas," *J. Solid State Electrochem.*, **8** 611-17 (2004).
28. B. Wang, B. Zydorczak, D. Poulidi, I.S. Metcalfe, and K. Li, "A Further Investigation of the Kinetic Demixing/decomposition of $La_{0.6}Sr_{0.4}Co_{0.2}Fe_{0.8}O_{3-\delta}$ Oxygen Separation Membranes," *J. Membrane Science*, **369** 526-35 (2011).
29. M. Martin and H. Schmalzried, "Cobaltous Oxide in an Oxygen Potential Gradient: Morphological Stability of the Phase Boundaries," *Ber. Bunsenges. Phys. Chem.*, **89** 124-30 (1985).
30. P. Tigelmann and M. Martin, "Monte Carlo Simulation of Surface Structures During Oxide Reduction," *Physica A*, **191** 240-47 (1992).
31. F.A. Nicols, "Kinetics of Diffusional Motion of Pores in Solids," *J. Nucl. Mater.*, **30** 143-65 (1969).